scientific reports

Check for updates

OPEN

Determination of solid-liquid adhesion work on flat surfaces in a direct and absolute manner

Norbert Nagy

There is a long-standing need for a direct determination of solid-liquid work of adhesion due to its central role in several scientific and industrial fields. Here, a method is introduced to determine the value of adhesion work on flat surfaces directly, without the need of any model assumptions, and independently from uncertainties of contact angles. The presented method enables to determine the adhesion work separately both for advancing and receding situations. The directly measured adhesion work values were benchmarked successfully against the prediction of the Young–Dupré equation in the 0°–120° contact angle range. That is, the Young–Dupré equation was experimentally proven to be valid separately for both advancing and receding cases. The method provides an absolute, thermodynamic quantity, hence it is insensitive to the measurement parameters, moreover the resulting values can be used directly in further calculations.

Keywords Wetting, Adhesion, Contact angle, Surface free energy, Young-Dupré equation, Surface organic contamination

The need of the determination of solid-liquid adhesion work is as old as Dupré's definition of the reversible work of adhesion. In addition to its scientific importance, this quantity is a critical factor affecting product quality and performance in many industrial fields. In general, it plays crucial role if the liquid should completely cover a solid surface (e.g. coatings, paints, inks, lubricants, adhesives, pesticides) or, on the contrary, the liquid should not remain on the surface at all (liquid repellency, anti-icing, etc.).

According to Dupré's definition, the adhesion work is the reversible thermodynamic work required to separate unit area of two phases in contact. Applying this definition to solid and liquid phases, the solid-liquid adhesion work (W_a) can be written as

$$W_a \equiv \gamma_{LV} - (\gamma_{SL} - \gamma_{SV}) \tag{1}$$

where γ_{LV} is liquid's surface tension, γ_{SL} is solid-liquid interfacial tension, and γ_{SV} is the surface stress of the solid[1] (commonly referred to as surface free energy of the solid)[2]. The last two quantities cannot be measured directly. However, their difference is included in the Young equation, which describes the condition for equilibrium of the contact line at the solid-liquid-vapor interface:

$$\gamma_{SV} - \gamma_{SL} - \gamma_{LV} \cdot \cos\vartheta = 0 \tag{2}$$

where ϑ is the contact angle at the contact line. The combination of these two equations eliminates the unknown difference term and results in the Young–Dupré equation:

$$W_a = \gamma_{LV} \cdot (1 + \cos\vartheta) \tag{3}$$

which relates the measured contact angle to adhesion work[3].

Traditionally, the work of solid-liquid adhesion has been determined through the measurement of contact angle. This contact angle based approach is very convenient and effective, however, it raises several questions. (a) Can the equilibrium contact angle be calculated from advancing and receding values and which one should be used in Eq. (3)? (b) What are the implications of a constantly changing receding contact angle, e.g. often on polymer surfaces? (c) What is the solution if the accuracy of contact angle measurement is not high enough[4]? The answers in short: (a) the advancing and receding contact angles together characterize the solid-liquid

Institute of Technical Physics and materials Science, HUN-REN Centre for Energy Research, P.O. Box 49, 1525 Budapest, Hungary. email: nagy.norbert@ek.hun-ren.hu

interaction, hence the Young contact angle should not be calculated and used in Eq. (3)[5,6]. (b) If the receding contact angle is not a definite value, the adhesion work is generally calculated from the advancing contact angle only. As a result, the solid-liquid adhesion work is underestimated and the liquid retention of the solid surface cannot be characterized[7]. (c) As high contact angles can only be measured with high uncertainty by sessile drops, novel methods and devices have been developed that measure the adhesion force between a solid and a liquid[8–11].

In ring based adhesion force measurements, a special ring holds a drop of water of a given volume. The ring is connected to an electromechanical microbalance. The investigated solid surface is lifted up until the liquid bridge is formed. The force measured at this moment is called snap-in force and it corresponds to the advancing contact angle[8,9]. The approach continues and then then the sample is moved down. During the retraction, the maximum magnitude of the measured force refers to the most stable contact angle[10]. The pull-off force is measured just before breakage of the liquid bridge. Its value correlates to the receding contact angle. The recent developments and results were reviewed carefully in ref[5]. In another similar technique – the scanning droplet adhesion microscope – the water drop is hold by a hydrophilic disk connected to a high resolution force sensor[11]. The volume of the disk attached drop can be adjusted in pL steps.

It is important to emphasize, that these methods allow only relative, comparative measurements, the value of the adhesion work cannot be directly obtained. For instance, the snap-in and pull-off forces determined on different solid surfaces are compared to decide which surface is more hydrophobic[12]. Such comparison can only be accurate if the drop volume and the minimal bridge length are exactly equal for all investigated surfaces.

As an alternative technique, the centrifugal adhesion balance was developed that aims the realization of Dupré's gedanken experiment, that is removing the liquid from a unit surface. The solid sample with a sessile drop is rotated with increasing angular velocity and it is tilted so that the resultant force is perpendicular to the sample's plane, until the solid-liquid contact line starts to shrink spontaneously. The solid-liquid adhesion work is calculated from the pull-off force and pull-off diameter in analogously to Tate law only for receding situation[13,14].

Capillary bridges are liquid bridges between two solid surfaces. They can be categorized based on boundary conditions. Between indefinite parallel plates, the boundary condition is the contact angle formed on the solid surfaces (θ bridges). Between circular plates, if the triple line pins at the circumference, the boundary condition is the radius of the disks (r bridges)[15]. In the last years, mainly capillary forces of θ liquid bridges were investigated and modelled between different solid surfaces[16–18] with contact angle hysteresis[19–22]. Liquid drop transfer was also studied[23,24] due to its central role in printing processes[25]. If the surface forces overwhelm the gravitational force, the axisymmetric capillary bridges have constant curvature surface and their possible shapes were classified by Plateau based on their dimensionless capillary pressure. For these Plateau-classes, the Young–Laplace equation can be solved analytically[17,26], in contrary to sessile drops[27]. Therefore, from the radii of the upper and lower contact line, the radius of the neck/haunch, and the capillary force, all parameters of a capillary bridge can be calculated including its length, volume, surface area, contact angles, and shape. However, all inverse problems are difficult to solve[28,29].

Recently, the Capillary Bridge Probe (CBP) method was introduced that allows precise contact angle determination in the entire contact angle range based on the measured capillary force and two geometrical parameters of the liquid bridge[30,31]. In this work, it is shown that using this technique, direct and absolute determination of the solid-liquid adhesion work is possible as well.

Measurement and evaluation

As test liquid, ultrapure water (resistivity: 18.2 MΩ cm; surface tension $\gamma_{water} = 72.25$ mN/m at 24 °) was used. The same experimental setup was used as previously for contact angle measurements, the detailed description of which can be found in Ref[30]. Briefly, the setup is similar to a contact angle goniometer arrangement: homogeneous light source, closed sample chamber with closed-to-saturated vapor of the test liquid (RH ≥ 85%), and a zoom objective with a CMOS camera (1280 × 1024 pixels, spatial resolution: 3.3 µm/pixel). A glass cylinder (diameter: 2 mm) with polished base plate is hooked on a force balance (resolution: 0.1 µN), which is mounted on a precise vertical actuator operated by a closed loop stepper motor (encoder resolution: 50,000 counts/rev).

In Fig. 1a, the measurement process is summarized: a capillary bridge of the test liquid is stretched between the base plate of the glass cylinder and the investigated solid surface, starting from a pendant drop. As the bridge length is decreased and then increased, the contact line advances and recedes on the solid surface, while the upper contact line remains pinned to the cylinder's rim. The cylinder is moved continuously with the velocity of 0.0025 mm/s, and the velocity of the contact line remains typically below 0.002 mm/s (quasi-static regime)[24,32,33]. During the change of separation distance between the cylinder and the solid surface, the image of the liquid bridge is captured in every fifth second, while the measured capillary force and the motor's position are recorded with the sampling rate of 2 Hz. Figure 1b shows a typical measured curve with hysteresis for the case of a stoichiometric Si_3N_4 surface. The insets show characteristic images of the water bridge, as examples.

Contact angle determination

For contact angle determination, the evaluation of a measurement cycle is performed according to the analytical description of capillary bridges mentioned in the Introduction. The detailed description of the image analysis and the whole evaluation process can be found in Ref[30,31]. In brief, the necessary geometrical bridge parameters are determined by the computer analysis of the captured image based on the Sobel method[34], while the corresponding capillary force is measured by the force balance. The contact angle, the bridge length, and the generatrix of the bridge profile are calculated from the measured value of the capillary force, neck/haunch radius, and radius of the contact line on the solid surface for each measured state. The difference between the generatrix and the real profile, and the difference between the measured and calculated bridge length indicate any deviation

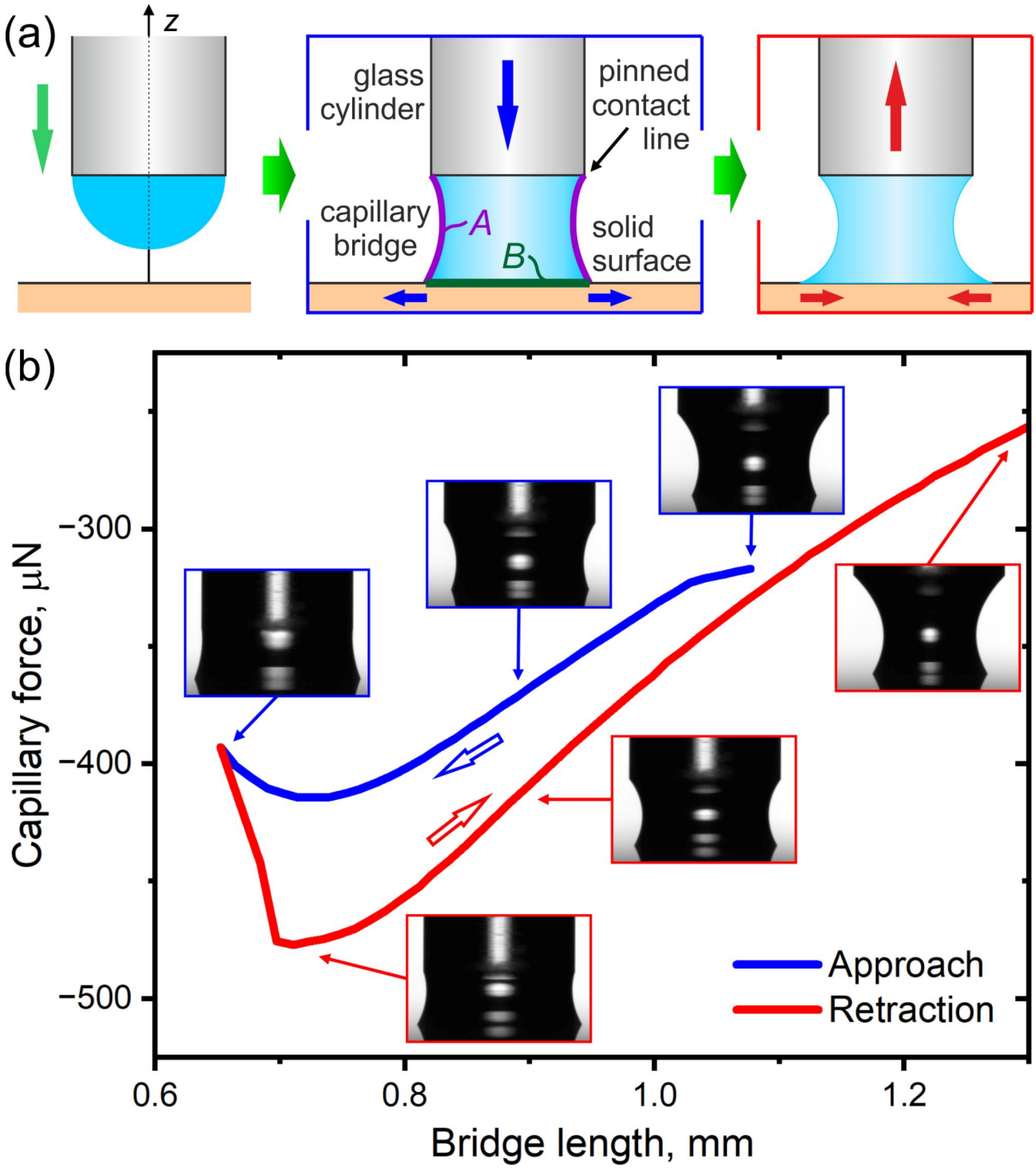

Fig. 1. (**a**) Schematics of the measurement steps. The liquid bridge is formed from a pedant drop. The contact line advances and recedes on the investigated surface, as the bridge length is decreased and then increased. During the length change, the image of the liquid bridge is captured and the capillary force is measured. The *z* axis is the axis of cylindrical symmetry. (**b**) Capillary force as a function of the bridge length measured on a hydrophilic (Si_3N_4) surface. The insets show captured images of the water capillary bridge. The diameter of the cylinder is 2 mm.

from the equilibrium state of an axisymmetric capillary bridge in the absence of gravity. Therefore, the bridge length can be also used as a sensitive control parameter during the evaluation: if their relative difference exceeds 4%, the measured point is neglected[30,31].

Adhesion work determination

The adhesion work can be measured by the present method without the need for any analytic evaluation. The measured quantities of capillary force, bridge length, and interfacial areas of the liquid bridge are the only needed parameters. However, the previously mentioned profile matching and the control parameter ensure the reliability of the results. The interfacial area between the test liquid and the solid surface (B) is calculated from the contact line diameter determined by image analysis, assuming cylindrical bridge symmetry. The interfacial area between the liquid and the fluid medium (A) is calculated as the mean area of surface of revolution of the left and right profile of the capillary bridge's image. That is the method is very simple in axisymmetric cases. For samples with strong and large scale lateral heterogeneity, the liquid bridge may tilt due to asymmetric contact line pinning. In this case, additional evaluation might be required. Furthermore, large scale lateral heterogeneity can cause inaccuracy of adhesion work due to the deviation of contact line from the perfect circular shape. However, due to the macroscopic scale of the liquid bridge, a small-scale chemical heterogeneity cannot cause significant error until their characteristic lateral dimension does not exceed the nanometer / sub-micrometer size range. In these cases, the contribution of the fine structure of the contact line to the area B should be negligible compared to the mm^2-scale interfacial area.

The mechanical work done on/by the system is calculated by numerical integration of the force-displacement curve, from which the work of adhesion can be determined, as described in the next section in detail.

Method for determination of adhesion work

During a measurement cycle of capillary bridge probe, the capillary force is measured as a function of the change of bridge length that is as a function of the vertical displacement of the cylinder. The direction of the net force coincides with the axis of cylindrical symmetry (z axis) and with the direction of the cylinder's displacement. That is the capillary force and the displacement have only z-component. Therefore, the presented method measures the mechanical work done on/by the system during one measurement. With this method, the value of this mechanical work can be determined separately for the advancing (approach) and receding (retraction) phases. This work is only spent on changing the interfacial areas, if gravitational force is negligible. During approach and retraction, both the area of the liquid-vapor interface (A) and that of the solid-liquid interface (B) change. Consequently, the energy balance can be written as

$$\Delta A \cdot \gamma_{LV} + \Delta B \cdot (\gamma_{SL} - \gamma_{SV}) = 0 \tag{4}$$

where $\overrightarrow{F}$ is the measured capillary force, $\overrightarrow{z}$ is the displacement of the cylinder, ΔA is the change of interfacial area between the liquid and vapor phase, and ΔB is the area change between the solid and the liquid. Obviously, the value of ΔA and ΔB are also dependent on the start and end points of the interval (z-range), over which the integration is performed. After rearranging Eq. (4), the difference term in the bracket can be expressed as:

$$(\gamma_{SL} - \gamma_{SV}) = -\frac{\int \overrightarrow{F}\overrightarrow{dz} + \Delta A \cdot \gamma_{LV}}{\Delta B}. \tag{5}$$

One can substitute this experimentally otherwise unattainable term into the definition of adhesion work (Eq. 1). Furthermore, considering that the net force and the displacement have only z-component, the vector notation can be omitted. This resulting formula gives the value of the solid-liquid adhesion work without the need of including any contact angle in the equation:

$$W_a = \gamma_{LV} + \frac{\int F dz + \Delta A \cdot \gamma_{LV}}{\Delta B}. \tag{6}$$

Integration between the start and end points of approach and retraction gives the mechanical work done in the advancing and receding phases, respectively. The change of interfacial areas can be determined by simple image analysis in cylindrically symmetric case. Therefore, the solid-liquid adhesion work can be calculated according to Eq. (6) for both the advancing and receding contact lines.

It has to be stressed, that the above presented approach determines the adhesion work directly, independently from contact angles and their uncertainties. The resulting quantity is an absolute one, hence its value is insensitive to measurement parameters like applied liquid volume and minimal bridge length. In advancing situation, it quantifies the driving force behind spreading of the test liquid on the solid surface. In receding situation, it is equal to the amount of work required to remove the liquid from a unit of solid surface.

The value of adhesion work should be also insensitive to the chosen z-range over which the integration is performed in Eq. (6). However, accuracy will be higher when an appropriate z-range is chosen, in which the contact line moves significantly, leaving out from the calculation those z-regions where only or mainly the liquid-vapor interfacial area has changed. The appropriate z-region can be easily selected by plotting the capillary force as a function of the contact radius. As an example, such a selection is shown in Fig. 2a for the same measurement as in Fig. 1b. Within this range, multiple and arbitrary combinations as the start and end points can be selected for evaluation. For each of these combinations, the adhesion work can be calculated individually. Note that for each case the actual start and end points of the integration are different, just like the corresponding mechanical work and the change of interfacial areas (ΔA and ΔB).

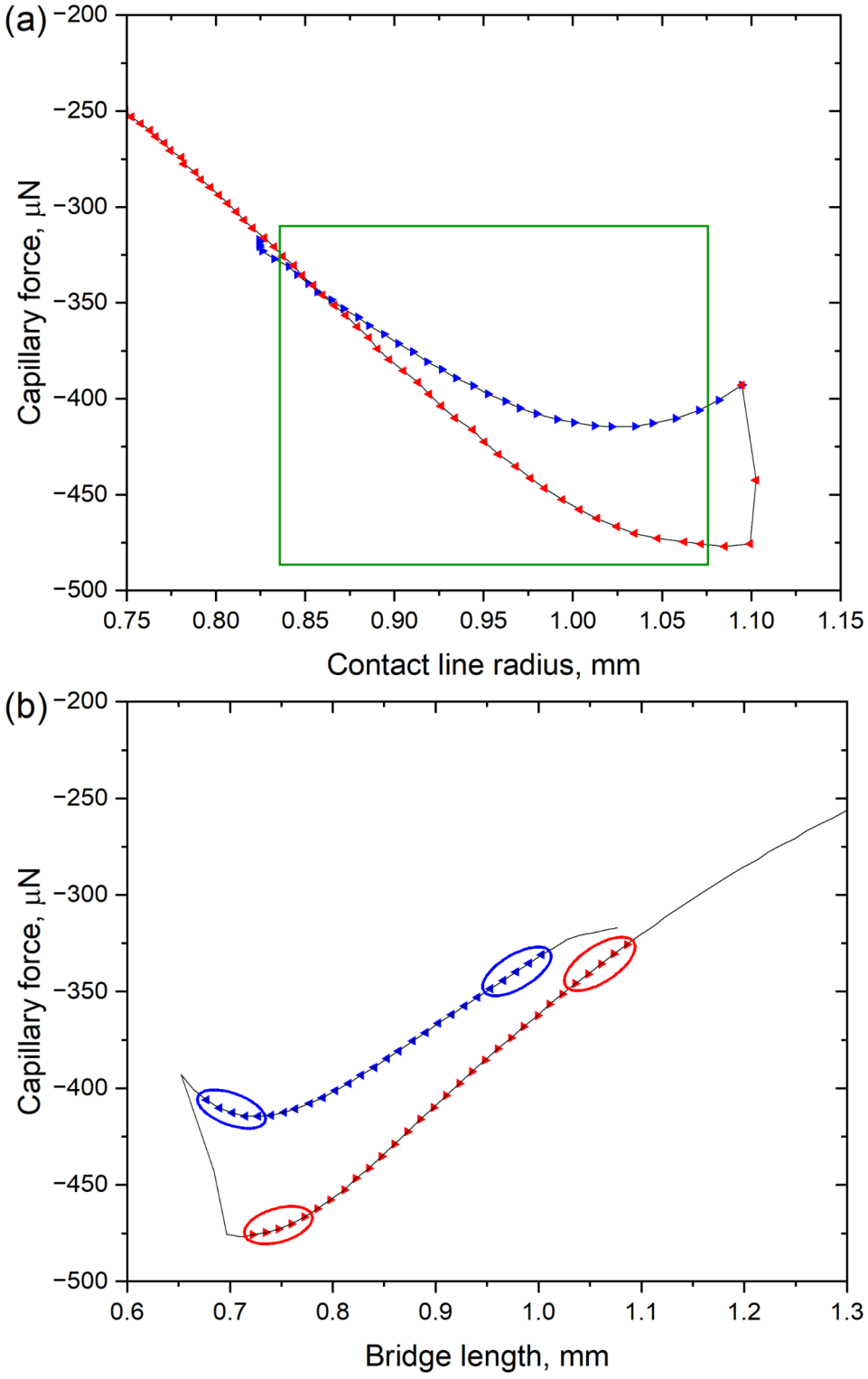

Fig. 2. (**a**) Illustrative example for the selection of the integration interval: capillary force is plotted as a function of the contact line radius measured on a clean Si_3N_4 surface (shown in Fig. 1b). The appropriate integration interval (z-region) is where the contact line moves significantly. Such a region is indicated by the green rectangle. Note, that the appropriate limits are not necessarily the same for the advancing and the receding situation. (**b**) In the selected interval, capillary force is plotted as a function of the bridge length. The 5–5 adjacent points are designated which were selected as start and end points of the integral for individual adhesion work calculations, for both advancing and receding situation. Note, that different ΔA and ΔB values corresponds to different start and end point pairs.

The results shown in this work were obtained by selecting 5–5 adjacent points from the beginning and end of the selected z-range (Fig. 2b) and their 25 combinations evaluated separately. Therefore, the presented adhesion work values are the average of 25 independent evaluation. Ideally, they should be equal, therefore their standard deviation refers to the surface homogeneity, e.g. in case of stick-slip motion of the contact line.

It is worth also mentioning that the method is mistake proof: in contrast to the error often made when measuring the receding contact angle, as for a stationary (pinned) contact line $\Delta B = 0$, Eq. (6) is not interpreted at this value.

Results of validation

For the validation, a sample series of different materials was selected to cover the 0°-120° contact angle range. The sample series contains dielectrics (glass, SiO_2, Si_3N_4), semiconductors (Si, mesoporous TiO_2), metals (Al, carbon steel), and polymers (COP, PTFE) with different surface conditions (clean, contaminated, acid- and plasma-treated). These surfaces were measured using ultrapure water with surface tension of $\gamma_{water} = 72.25$ mN/m as test liquid. To obtain contaminated surfaces, surface organic contamination was allowed to accumulate on the sample surface during their storage in closed sample boxes placed in a closed laboratory cabinet for at least 3 months. See Experimental section for details.

In Fig. 3, the directly measured adhesion work values were plotted. The blue and red points represent the work of adhesion measured in the advancing and receding phase, respectively. The green points were measured in readvancing situation. This readvancing effect can be observed in case of perfect wetting: the receding contact line start to advance again during the retraction of the cylinder. (The readvancing contact line already finds wetted surface in front of it, hence the measured contact angle is lower than in the receding situation, its value is typically $\leq 1°$.)[30] The corresponding vertical error bars show the standard deviation of the directly measured adhesion work values determined according to the above-described procedure. The adhesion work values were plotted as a function of contact angle, of which values were measured during the same capillary bridge probe measurement and obtained by analytic evaluation as described previously. The horizontal error bars show their standard deviation. The tabulated data of Fig. 3 can be found in Table S1.

A general cosine function was fitted to all of these measured points:

$$W_a(\vartheta) = \gamma \cdot (1 + q \cdot \cos\vartheta) \tag{7}$$

where γ and q are fitting parameters. The purple curve represents the result of this fit. The resulted values of the fitting parameters are $\gamma = 72.5 \pm 0.2$ and $q = 1.008 \pm 0.006$. The fitted value of γ is in good agreement with the measured surface tension of the test liquid, while the value of q is practically equal to one, as expected.

For comparison, the theoretical curve of the Young–Dupré equation was also plotted as the dashed green curve, according to Eq. (3), into which the surface tension of the test liquid (γ_{water}) was substituted as γ_{LV}. The fitted cosine curve is in perfect match with the curve corresponding to the Young–Dupré equation.

As a consequence, accurately measured advancing and receding contact angles can be used to calculate the adhesion work for the two different situations. It is worth to note that the calculation of adhesion work from the Young–Dupré equation relies on the precise measurement of the contact angle. When for instance, the directly measured adhesion work is plotted against the sessile drop contact angles, the correlation is of much lower quality (Figure S1). Furthermore, in accordance with the previous consequence, this direct method provides an additional advantage: if the receding contact angle is not a stationary definite value, an effective receding contact angle can be calculated from the measured adhesion work using the Young–Dupré equation.

Conclusion

In conclusion, the method determines the solid-liquid adhesion work directly and both for advancing and receding scenarios without any model assumptions. In advancing situation, the adhesion work quantifies the driving force behind spreading, while it gives the work required to remove the liquid from a unit of solid surface in receding case. The Young–Dupré equation was proved to be valid separately for advancing and receding situations. The method works in the entire contact angle range, and high energy surfaces can be characterized without prewetting, in contrary to the captive bubble method. The presented method provides an absolute, thermodynamic quantity, hence it is insensitive to the measurement parameters, and furthermore the resulting values can be used directly for further calculations, e.g. in the various surface free energy models. The method can be applied easily using commercial tensiometers equipped with an optional commercial camera module or with a laboratory-built one.

Experimental section

Measurement method

All measurements were carried out in close-to-saturated water vapor (RH $\geq$ 85%) at 24 °C.

Before the measurement, a pendant drop is formed on the base plate of the glass cylinder and its initial volume is determined with the precision of 0.01 µL. It approaches the sample surface and after the bridge formation (snap-in), the cylinder is lowered continuously (0.0025 mm/s). The velocity of the contact line remains typically below 0.002 mm/s (quasi-static regime)[24,32,33]. The decrease of the bridge length is terminated at a chosen bridge length, contact radius, or capillary pressure. Then, the bridge length is being increased (retraction phase) with the same velocity until the breakage of the bridge (pull-off). The image of the capillary bridge is captured in every fifth second, while the measured capillary force, and the motor's position are recorded with the sampling rate of 2 Hz.

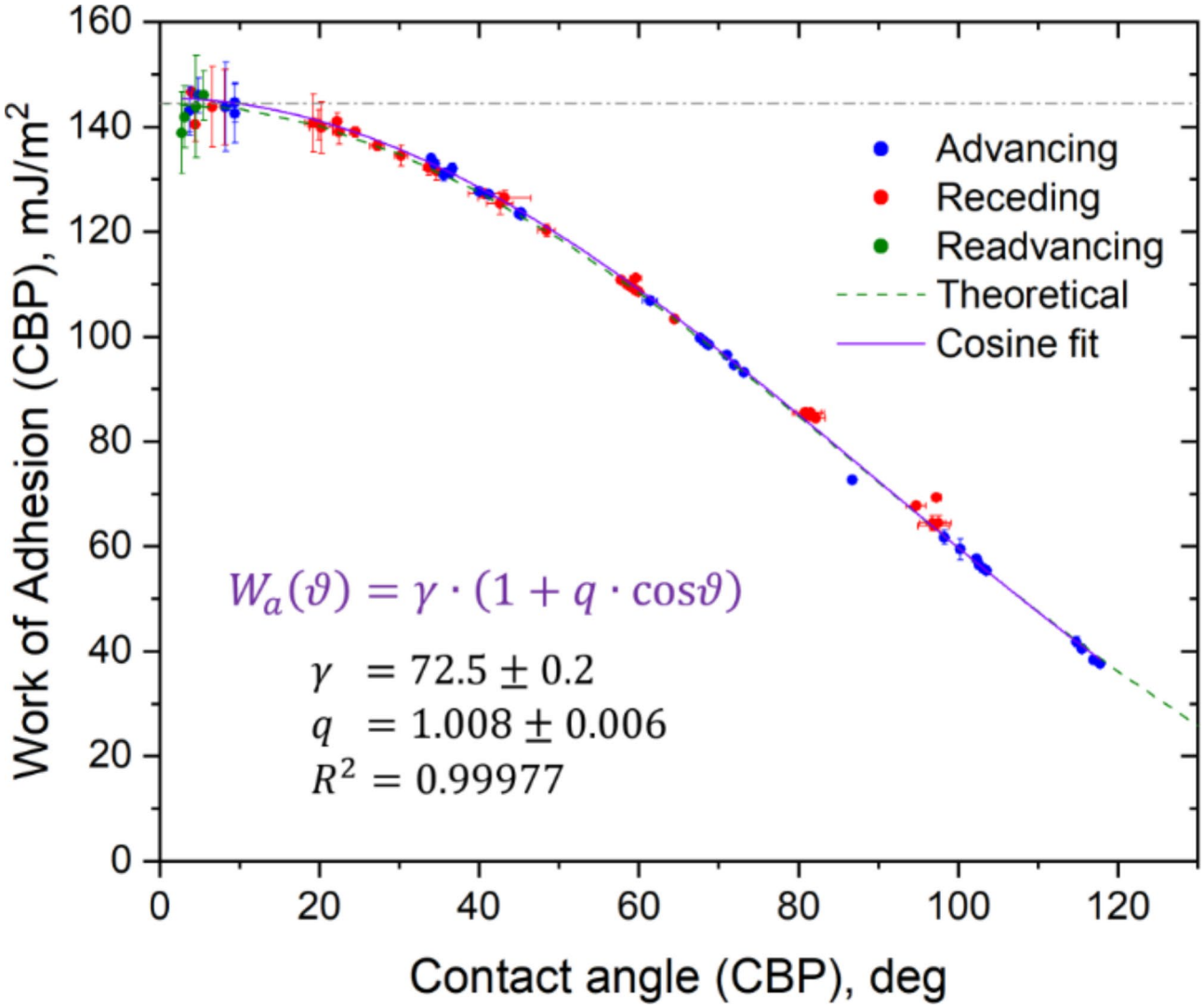

Fig. 3. Directly measured adhesion work values are plotted as blue, red, and green points for advancing, receding, and readvancing situation, respectively, as a function of contact angle. Contact angle values were determined during the same capillary bridge probe (CBP) measurement. The inset shows the result of the fit of a general cosine function to all measurement points. The fitted purple curve is in excellent agreement with the theoretical dashed green curve corresponding to the Young–Dupré equation. For this validation, metal, semiconductor, dielectric, and polymer surfaces were measured in clean, contaminated, acid-, and plasma-treated condition using ultrapure water as test liquid.

Evaluation

The interfacial area between the test liquid and the solid surface (B) is calculated from the contact diameter determined by image analysis, supposing cylindrical symmetry. The interfacial area between the liquid and the fluid medium (A) is calculated as the mean area of surface of revolution of the left and right profile of the capillary bridge's image. The mechanical work is calculated by numerical integration of the force-displacement curve. For every evaluation, 5–5 adjacent measurement points were chosen as start and end points of the integration interval, hence the presented adhesion work values are the mean of 25 independently calculated values.

Materials

Test liquid: Ultrapure water purified by a Sartorius Arium Mini ultrapure water system; resistivity: 18.2 MΩ·cm; surface tension $\gamma_{water} = 72.25$ mN/m at 24 °C measured by Wilhelmy balance method (KSV 2000) and pendant drop method (Krüss DSA 30).

Cleaning materials: Acetone (≥ 99.8%, ACS Reag. Ph. Eur., VWR Chemicals); Ethanol absolute (≥ 99.8%, ACS Reag. Ph. Eur., VWR Chemicals); Sulphuric acid (≥ 96%, Carlo Erba); Hydrogen peroxide (30%, a.r., Reanal); ultrapure water (purified by a Sartorius Arium Mini system; resistivity: 18.2 MΩ·cm); Piranha solution (1:3 H_2O_2:H_2SO_4, prepared freshly in cooling bath).

Samples

Silicon wafers: (100), p-type, 1–30 Ω·cm, prime grade (Siegert).

The thermal SiO_2 and chemical vapor deposited stoichiometric Si_3N_4 layers were grown in the cleanroom laboratory of the Institute of Technical Physics and Materials Science at HUN-REN Centre for Energy Research. The aluminium film with the thickness of ca. 1 μm was deposited by vacuum evaporation onto Si substrate, as well. These (clean) samples were measured as received. They were rinsed with ultrapure water and dried under gentle, dry, filtered (0.01 μm, Kitz Unipore air gun) nitrogen flow after the measurements[30].

The stainless steel (1.4571; 316Ti) surface was polished on a metallurgical polishing machine to mirror finish and cleaned thoroughly in methanol. It was measured as received[35].

Microscope glass slides (Menzel-Gläser, 76 × 26 × 1 mm (Thermo Scientic)) were cleaned in acetone, ethanol, and ultrapure water. Samples were dipped in sulfuric acid or Piranha solution for 5 min and 30 min, respectively, then rinsed thoroughly with ultrapure water and stored in degassed ultrapure water until the measurements. Other clean glass slides were plasma-cleaned in a Harrick plasma cleaner for 5 min and stored in degassed ultrapure water until the measurements.

Cyclo Olefin Polymer (Zeonex® 480R) was dissolved in toluene (1 m/V %) and spin-coated onto microscope cover slides (Menzel-Gläser) at 3000 rpm[31].

Mesoporous titania thin film was prepared by sol-gel method and deposited onto Si substrate by spin coating. The micelle-forming template molecules (Pluronic P123) were removed by thermal treatment for 1 h at 480 °C[36].

Polytetrafluoroethylene sheets (PTFE; Kolo Ltd., Hungary) with the thickness of 1 mm were polished to remove the surface strips caused by rolling using 800–2000 Grit polishing sheets. Then the PTFE samples were hot pressed between microscope glass slides (Menzel-Gläser) at ca. 210 °C for ca. 1.5 h. Finally, the surface became glossy in general, however containing microscopic imperfections (pits)[31].

Surface organic contamination (SOC) was accumulated on the sample surfaces during their storage in closed sample boxes placed in a closed laboratory cabinet for at least 3 months. During this time, the organic contamination became saturated[37–41]. Interestingly, this accumulated organic thin films are virtually undetectable even by spectroscopic ellipsometry (Woollam M-2000). As an example, the measured and fitted ellipsometric spectra of the SOC-coated Si_3N_4 film and the difference in ellipsometric spectra between the clean and contaminated Si_3N_4 film are shown in Figure S2a and b, respectively. The effective layer thickness changed from 128.9 ± 0.07 nm (MSE: 12.65) to 129.2 ± 0.02 nm (MSE: 13.37), while the advancing water contact angle increased from 40 ± 0.1° to 68.8 ± 0.1° and the receding contact angle increased from 27.2 ± 0.9° to 60 ± 0.1°.

Data availability

Data is provided within the manuscript and supplementary information file.

Received: 26 June 2024; Accepted: 28 November 2024
Published online: 02 December 2024

References

1. Erbil, H. Y. *Surface Chemistry of Solid and Liquid Interfaces* (Blackwell Pub, 2006).
2. Possart, W. & Shanahan, M. E. R. Thermodynamics of adhesion. in Handbook of Adhesion Technology (eds Da Silva, L. F. M., Öchsner, A. & Adams, R. D.) 105–116 (Springer, Berlin, 2011) https://doi.org/10.1007/978-3-642-01169-6_6.
3. Van Oss, C. J. The apolar and polar properties of liquid water and other condensed-phase materials. in *Interface Science and Technology* vol. 16 13–30 (Elsevier, 2008).
4. Liu, K., Vuckovac, M., Latikka, M., Huhtamäki, T. & Ras, R. H. A. improving surface-wetting characterization. *Science* **363**, 1147–1148 (2019).
5. Drelich, J. W. Contact angles: From past mistakes to new developments through liquid-solid adhesion measurements. *Adv. Colloid Interface Sci.* **267**, 1–14 (2019).
6. Drelich, J. W. et al. Contact angles: History of over 200 years of open questions. *Surf. Innov.*. **8**, 3–27 (2020).
7. Bormashenko, E. Wetting of real solid surfaces: New glance on well-known problems. *Colloid Polym. Sci.* **291**, 339–342 (2013).
8. Samuel, B., Zhao, H. & Law, K. Y. Study of wetting and adhesion interactions between water and various polymer and superhydrophobic surfaces. *J. Phys. Chem. C.* **115**, 14852–14861 (2011).
9. Sun, Y. et al. Direct measurements of adhesion forces for water droplets in contact with smooth and patterned polymers. *Surf. Innov.*. 1–52. https://doi.org/10.1680/jsuin.17.00049 (2017).
10. Sun, Y. et al. The most stable state of a droplet on anisotropic patterns: Support for a missing link. *Surf. Innov.* **6**, 133–140 (2018).
11. Liimatainen, V. et al. Mapping microscale wetting variations on biological and synthetic water-repellent surfaces. *Nat. Commun.* **8**, 1798 (2017).
12. Hokkanen, M. J., Backholm, M., Vuckovac, M., Zhou, Q. & Ras, R. H. A. Force-based wetting characterization of stochastic superhydrophobic coatings at nanonewton sensitivity. *Adv. Mater.* **33**, 2105130 (2021).
13. Tadmor, R. et al. Solid–liquid work adhes. *Langmuir* **33**, 3594–3600 (2017).
14. Extrand, C. W. Comment on solid–liquid work of adhesion. *Langmuir* **33**, 9241–9242 (2017).
15. Fortes, M. A. Axisymmetric liquid bridges between parallel plates. *J. Colloid Interface Sci.* **88**, 338–352 (1982).
16. De Souza, E. J., Brinkmann, M., Mohrdieck, C., Crosby, A. & Arzt, E. Capillary forces between chemically different substrates. *Langmuir* **24**, 10161–10168 (2008).
17. Wang, Y., Michielsen, S. & Lee, H. J. Symmetric and asymmetric capillary bridges between a rough surface and a parallel surface. *Langmuir* **29**, 11028–11037 (2013).
18. Coelho, R. C. V., Cordeiro, L. A. R. G., Gazola, R. B. & Teixeira, P. I. C. Dynamics of two-dimensional liquid bridges. *J. Phys.: Condens. Matter.* **34**, 205001 (2022).
19. Chen, H., Amirfazli, A. & Tang, T. Modeling liquid bridge between surfaces with contact angle hysteresis. *Langmuir* **29**, 3310–3319 (2013).
20. De Souza, E. J., Gao, L., McCarthy, T. J., Arzt, E. & Crosby, A. J. Effect of contact angle hysteresis on the measurement of capillary forces. *Langmuir* **24**, 1391–1396 (2008).
21. Shi, Z., Zhang, Y., Liu, M., Hanaor, D. A. H. & Gan, Y. Dynamic contact angle hysteresis in liquid bridges. *Colloids Surf. A: Physicochem. Eng. Asp.* **555**, 365–371 (2018).

22. Odunsi, M. S., Morris, J. F. & Shattuck, M. D. Hysteretic behavior of capillary bridges between flat plates. *Langmuir* **39**, 13149–13157 (2023).
23. Chen, H., Tang, T. & Amirfazli, A. Liquid transfer mechanism between two surfaces and the role of contact angles. *Soft Matter.* **10**, 2503 (2014).
24. Chen, H., Tang, T., Zhao, H., Law, K. Y. & Amirfazli, A. How pinning and contact angle hysteresis govern quasi-static liquid drop transfer. *Soft Matter*. **12**, 1998–2008 (2016).
25. Kumar, S. Liquid transfer in printing processes: Liquid bridges with moving contact lines. *Annu. Rev. Fluid Mech.* **47**, 67–94 (2015).
26. Kralchevsky, P. A. & Nagayama, K. Capillary bridges and capillary-bridge forces. in *Studies in Interface Science* vol. 10 469–502 (Elsevier, (2001).
27. Rotenberg, Y., Boruvka, L. & Neumann, A. W. Determination of surface tension and contact angle from the shapes of axisymmetric fluid interfaces. *J. Colloid Interface Sci.* **93**, 169–183 (1983).
28. Gagneux, G. & Millet, O. Analytic calculation of capillary bridge properties deduced as an inverse problem from experimental data. *Transp. Porous Med.* **105**, 117–139 (2014).
29. Lian, G. & Seville, J. The capillary bridge between two spheres: new closed-form equations in a two century old problem. *Adv. Colloid Interface Sci.* **227**, 53–62 (2016).
30. Nagy, N. Contact angle determination on hydrophilic and superhydrophilic surfaces by using *r* –θ-type capillary bridges. *Langmuir* **35**, 5202–5212 (2019).
31. Nagy, N. Capillary bridges on hydrophobic surfaces: Analytical contact angle determination. *Langmuir* **38**, 6201–6208 (2022).
32. Restagno, F., Poulard, C., Cohen, C., Vagharchakian, L. & Léger, L. Contact angle and contact angle hysteresis measurements using the capillary bridge technique. *Langmuir* **25**, 11188–11196 (2009).
33. Cohen, C., Restagno, F., Poulard, C. & Léger, L. Wetting and dewetting transition: An efficient toolbox for characterizing low-energy surfaces. *Langmuir* **26**, 15345–15349 (2010).
34. Canny, J. A. Computational approach to edge detection. *IEEE Trans. Pattern Anal. Mach. Intell. PAMI* **8**, 679–698 (1986).
35. Pfeifer, É. K., Gyurika, I. G. & Telegdi, J. Anticorrosion activity of phosphonic acid amphiphile in self-assembled molecular layer. *Int. J. Corros. Scale Inhib.* **12** (2023).
36. Tegze, B. et al. Effect of silver modification on the photoactivity of titania coatings with different pore structures. *Nanomaterials* **11**, 2240 (2021).
37. Ishiwari, S., Kato, H. & Habuka, H. Development of evaluation method for organic contamination on silicon wafer surfaces. *J. Electrochem. Soc.* **148**, G644 (2001).
38. Habuka, H., Ishiwari, S., Kato, H., Shimada, M. & Okuyama, K. Airborne organic contamination behavior on silicon wafer surface. *J. Electrochem. Soc.* **150**, G148 (2003).
39. Tlili, S., Hayeck, N., Gligorovski, S. & Wortham, H. Adsorption features of phthalates and organophosphorus compounds on silicon wafers. *Ind. Eng. Chem. Res.* **51**, 14665–14672 (2012).
40. Hurst, J. M., Kim, M. A., Peng, Z., Li, L. & Liu, H. Assessing and mitigating surface contamination of carbon electrode materials. *Chem. Mater.* **31**, 7133–7142 (2019).
41. Pálinkás, A. et al. The composition and structure of the ubiquitous hydrocarbon contamination on Van Der Waals materials. *Nat. Commun.* **13**, 6770 (2022).

Acknowledgements

Support from the National Development Agency Grants of OTKA Nr. FK 128901 and K 146181 is greatly acknowledged. Project no. TKP479 2021-EGA04 has been implemented with the support from the Ministry of Innovation and Technology of Hungary from the National Research, Development and Innovation Fund, financed under the TKP2021 funding scheme. The author thanks A Deák, B Tegze, Cs. Dücső, J. Telegdi for the high-quality samples, and Plósz Engineering Ltd. for the excellent manufacturing.

Author contributions

N.N. carried out all measurements, performed all calculations, evaluated and analyzed all measurement data and then wrote the manuscript text, discussed the results, and reviewed the manuscript.

Declarations

Competing interests

Author is the inventor, HUN-REN Centre for Energy Research is the applicant of the related patent application.

Additional information

Supplementary Information The online version contains supplementary material available at https://doi.org/10.1038/s41598-024-81710-6.

Correspondence and requests for materials should be addressed to N.N.